Energy Conversion and Management: X 10 (2021) 100079

Contents lists available at ScienceDirect

Energy Conversion and Management: X

journal homepage: www.sciencedirect.com/journal/energy-conversion-and-management-x

Can methane pyrolysis based hydrogen production lead to the decarbonisation of iron and steel industry?

Abhinav Bhaskar *, Mohsen Assadi, Homam Nikpey Somehsaraei

University of Stavanger, 4036, Norway

ARTICLE INFO

Keywords:
Industrial decarbonisation
Hydrogen direct reduction
Methane Pyrolysis
Water electrolysis
Green steel

ABSTRACT

Decarbonisation of the iron and steel industry would require the use of innovative low-carbon production technologies. Use of 100% hydrogen in a shaft furnace (SF) to reduce iron ore has the potential to reduce emissions from iron and steel production significantly. In this work, results from the techno-economic assessment of a H_2-SF connected to an electric arc furnace(EAF) for steel production are presented under two scenarios. In the first scenario H_2 is produced from molten metal methane pyrolysis in an electrically heated liquid metal bubble column reactor. Grid connected low-temperature alkaline electrolyser was considered for H_2 production in the second scenario. In both cases, 59.25 kgH_2 was required for the production of one ton of liquid steel (tls). The specific energy consumption (SEC) for the methane pyrolysis based system was found to be 5.16 MWh/tls. The system used 1.51 MWh/tls of electricity, and required 263 kg/tls of methane, corresponding to an energy consumption of 3.65 MWh/tls. The water electrolysis based system consumed 3.96 MWh/tls of electricity, at an electrolyser efficiency of 50 KWh/kgH_2. Both systems have direct emissions of 129.4 kgCO2/tls. The indirect emissions are dependent on the source of natural gas, pellet making process and the grid-emission factor. Indirect emissions for the electrolysis based system could be negligible, if the electricity is generated from renewable energy sources. The levellized cost of production(LCOP) was found to be $631, and $669 respectively at a discount rate of 8%, for a plant-life of 20 years. The LCOP of a natural gas reforming based direct reduction steelmaking plant of operating under similar conditions was found to be $414. Uncertainty analysis was conducted for the NPV and IRR values.

1. Introduction

Global greenhouse gas(GHG) emissions need to be reduced by 45% by 2030 from 2010 levels and to net zero by 2050 to limit global mean temperature rise to 1.5 °C [1]. Energy intensive industries (EII) like iron and steel, aluminum, cement, chemicals etc. are responsible for large share of the global GHG emissions. Decarbonisation of EII's is essential to achieve the 2050 emission reduction targets. Iron and steel production contributes to 7% of the global GHG emissions [2]. The use of demand reduction measures like material efficiency, material substitution and product service-life extension are important in achieving emission reductions from the steel industry [3]. However, in the short and medium term, as living standards improve in developing countries, the demand for steel could increase. The demand for primary steel is projected to increase by 30% in the next three decades [4]. At present majority of the primary steel is produced through the blast furnace-basic oxygen furnace(BF-BOF) route, where coke is used to reduce Fe_2O_3 to Fe in the BF and is converted to steel in the BOF. Approximately 1.8 ton(t) of CO_2 is released to produce ton of liquid steel (tls) [5]. An alternative production route is the reduction of solid Fe_2O_3 by a mixture of CO and H_2 in a direct reduction shaft furnace [6]. The direct reduced iron (DRI) could be processed in an electric arc furnace (EAF) to produce steel. The reducing gas is produced from reforming of natural gas or through coal gasification. The specific energy consumption (SEC) of a natural gas(NG) reforming based DRI-EAF systems varies from 2.9–3.5 MWh/tls, and direct emissions vary from 0.9 to 1.2 tCO_2/tls [7]. Efficiency improvement measures have reduced the energy and emission intensity of the steel industry in the past decades. However, complete decarbonisation of the iron and steel industry, while meeting the increasing steel demand, would require the introduction of innovative production technologies [8,9].

Fischedick et al. evaluated the techno-economic feasibility of three innovative iron production technologies i.e. blast furnace with carbon capture and storage (CCS), low and high-temperature iron ore electrolysis (electrowining), and H_2-direct reduction (DR) [10]. They found

* Corresponding author.
E-mail address: abhinav.bhaskar@uis.no (A. Bhaskar).

https://doi.org/10.1016/j.ecmx.2021.100079

Available online 10 March 2021

Nomenclature

Following abbreviations were used in the manuscript

H_2-SF-EAF	Hydrogen-shaft furnace-electric arc furnace
DRI-EAF	Direct reduced iron-electric arc furnace
BF-BOF	Blast furnace-Basic oxygen furnace
SMR	Steam methane reforming
CCS	Carbon capture and storage
DR	Direct reduction
GHG	Green house gas
EII	Energy intensive industry
LTE	low-temperature electrolyser
HTE	High-temperature electrolyser
SMR	Steam methane reforming
BASF	Badische Anilin und Soda Fabrik
SSAB	Svenskt Stål AB
LKAB	Luossavaara-Kiirunavaara Aktiebolag
LMBR	Liquid metal bubble column reactor
PSA	Pressure swing adsorber
EAF	Electric arc furnace
HEX	Heat exchanger
SF	Shaft furnace
TRL	Technology readiness level
TDM	Thermal decomposition of methane
SEC	Specific energy consumption
MWh	Megawatt hour
KWh	Kilowatt hour
kJ	Kilojoule
MJ	Megajoule
MMBTU	Metric Million British Thermal Unit
$	US dollar
tls	Ton of liquid steel
kg	Kilogram
kgH_2	Kilogram of hydrogen
kt	Kiloton
Mt/y	Million ton per year
t	ton
kta^{-1}	Kiloton per annum
tCO_2	Ton of carbon dioxide
K	Kelvin
°C	Celsius
CF	Cash flow
NPV	Net present value
IRR	Internal rate of return
LCOP	Levellized cost of production
ACC	Annualized capacity factor or annuity factor
capex	Capital expenditure
opex	Operational expenditure
GEF	Grid emission factor
H_2	Hydrogen
O_2	Oxygen
H_2O	Water
CH_4	Methane
CO_2	Carbon dioxide
CO	Carbon Monoxide
N_2	Nitrogen
Fe	Iron
FeO	Iron oxide
Fe_2O_3	Iron oxide (Hematite)
Fe_3O_4	Iron oxide (Magnetite)
Al_2O_3	Alumina
SiO_2	Silica
CaO	Calcium oxide (lime)
MgO	Magnesium oxide
NG	Natural gas

that H_2-DR and electrolysis based production routes have the highest potential to decarbonise the steel industry in the future. A multi-criteria analysis of primary steelmaking technologies was conducted by Weigel et al. [11]. Electrolysis and H_2-DR were rated as the most promising technologies for low-carbon steel production. Toktarova et al. conducted a techno-economic pathway analysis for low-carbon transition of the Swedish steel industry. They found that H_2-DR-EAF based steel production has the highest decarbonisation potential and could reduce total CO_2 emissions in Sweden by 10% [12]. Under the Ultra-Low Carbon Dioxide Steelmaking (ULCOS) research program, two iron-ore electrolysis processes were studied [13,6]. These processes are still at lab-scale and are not expected to be available for commercial deployment before 2040, and are hence not included in this analysis [10]. DR of iron ore with 100% H_2 was carried out at commercial scale using fluidized-bed reactors at an industrial plant in Trinidad and Tobago in the early 1990's [14]. The plant produced steel with 95% metallization rate, at a production capacity of 65 ton of liquid steel per hour (tls/hr) in a shaft-furnace(SF) reactor [15]. Direct reduction with more than 90% H_2 was conducted by Energiron at a test facility in Hysla, Monterrey [16]. A H_2-(SF) plant with an output capacity of one ton/day was commissioned under the HYBRIT project (consortium of Luossavaara-Kiirunavaara Aktiebolag (LKAB), Svenskt Stål AB (SSAB), and Vattenfall) in August 2020 in Sweden [17]. The project also aims to the develop a fossil fuel free pellet making process and a H_2 storage unit for continuous functioning of the plant. All major steel companies are involved in building industrial demonstration plants for H_2-SF based plants [18–22]. The largest producers of DRI shaft furnces, MIDREX and ENERGIRON, have indicated that their shaft furnace designs can be easily modified to use 100% H_2 as the reducing agent [23,16].

H_2 required for steel production could be produced by water electrolysis or from fossil fuels like natural gas or coal. 95% of H_2 is produced by steam methane reforming (SMR) at present. However, SMR process has a high carbon-footprint, and it's continued use would be an obstacle in achieving the emission reduction goals. In recent times, the role of green H_2 produced from water electrolysis, using renewable electricity has become increasingly prominent in decarbonising the energy system. It has the potential to decarbonise hard-to-abate sectors like industries (steel, ammonia, methanol etc.), heavy transport, shipping and aviation [24]. Although renewable electricity powered water electrolysis produces emission-free H_2, limited availability, and high-prices of renewable electricity are a deterrent to the large-scale deployment of industrial decarbonisation projects [2,5]. For example, converting existing steel production units in the EU to H_2-SF-EAF would require an additional 300–400 TWh/year of renewable electricity [25]. In the short and medium term, low-carbon H_2 produced from natural gas could pave the way for industrial H_2 projects [23]. SMR coupled with carbon capture and storage (CCS) has been proposed as an alternative for low-carbon H_2 production. However, there are concerns about the cost, safety and social acceptability of CCS [26]. Another alternative for low-carbon H_2 production is methane pyrolysis, where CH_4 is decomposed to solid-carbon and CH_4 [27]. Methane pyrolysis could act as a bridge technology until large-amounts of cheap renewable electricity becomes available, while infrastructure and end-use applications are deployed [28]. Parkinson et al. evaluated the costs of carbon mitigation from a life-cycle perspective of 12 different hydrogen production technologies, and found methane pyrolysis as the most cost-effective short-term carbon abatement solution [29].

To the best of the knowledge of the authors, integration of methane

pyrolysis with H_2-SF-EAF system based steel production has not been evaluated previously. In this work, techno-economic assessment of H_2-SF-EAF system based steel production has been conducted for two scenarios. Iron ore reduction is carried out in a H_2-SF and an EAF is used for steelmaking in both cases. H_2 is produced from methane pyrolysis in the first scenario and water electrolysis in the second. The analysis was conducted to answer the following questions.

1. Is it techno-economically feasible to integrate methane pyrolysis with H_2-SF-EAF system based steel making process?
2. How does methane pyrolysis compare with water electrolysis based H_2-SF-EAF system system in terms of SEC, emissions, and economic parameters?
3. Which factors have the maximum impact on the economic performance of H_2-SF-EAF system based steel production systems in both the scenarios?

The rest of the paper is structured as following. A brief review of the literature is presented in Section 2. Section 3, describes the methodology used to develop the techno-economic assessment model. The modelling and simulation results of the analysis are presented in Section 4. Discussions and inferences from the analysis are collated in Section 5, followed by the conclusions in Section 6.

2. Literature review

Vogl et al. conducted a techno-economic analysis of H_2-SF-EAF based steel production route, a low-temperature electrolyser(LTE) was used for hydrogen generation [30]. Their assessment revealed that the production costs vary from €361–640/t of steel, and is highly dependent on the price of electricity and the carbon emission prices. In a recent article, Krüger et al. analyzed the techno-economics of integrating a high-temperature electrolyser(HTE) to the H_2-SF-EAF system [31]. They calculated a 21% reduction in the energy consumption of a HTE based system. Some researchers haves evaluated the use of methanol produced from co-electrolysis of H_2O and CO_2 in the shaft furnace for steel production [32].

Methane pyrolysis is an endothermic reaction and requires high-temperatures (1273–1773 K) to achieve high-conversion rates. Solid-carbon, produced as a by-product of methane pyrolysis has many industrial applications, and could be sold at $0.4/kg -$2/kg to generate additional revenue [33]. Excess unsold carbon could be stored in geological storage or unused coal mines [29]. It can be handled, transported and stored at a fraction of the cost of gaseous CO_2. Schneider et al. reviewed different technologies for production of H_2 from methane pyrolysis, thermal decomposition, plasma decomposition and catalytic decomposition. Keipi et al. compared the economic feasibility of hydrogen production by methane pyrolysis with SMR and water electrolysis. H_2 produced by pyrolysis was found to have the lowest specific CO_2 emissions, and the economic feasibility was found to be dependent on the market price of solid-carbon [27]. Monolith materials has commissioned a methane pyrolysis plant in Nebraska, United states, primarily for carbon-black production [34]. They intend to use the by-product H_2 for industrial scale low-carbon ammonia production. The company uses plasma decomposition process powered by renewable electricity [35].

High-temperatures required for pyrolysis leads to complex reactor designs and higher costs. Thermo-catalytic reduction of CH_4 could lower the reaction temperature, leading to simpler reactor design. Metallic catalysts, carbonaceous catalysts like activated carbon and carbon black have been investigated previously for the production of H_2 from methane pyrolysis [36]. High-conversion rates were achieved at temperaures lower than 1273 K, but deposition of carbon on the surface of the catalysts reduces their activity, and can clog the fluid-bed and packed-bed reactors used for thermo-catalytic conversion of CH_4 to H_2 and solid-carbon [37–39].

2.1. Molten metal methane pyrolysis

Molten metal pyrolysis, utilizes the low-density and insolubility of solid-carbon in liquids for effective separation of carbon, and could solve the problem of reactor clogging by carbon deposition [40]. CH_4 is passed through a molten metal in a liquid metal bubble column reactor(LMBR), decomposing it to solid-carbon and H_2. Serban et al. achieved a methane conversion of 57% using molten tin in a LMBR at 1023 K [41]. Several experimental studies have recorded high-conversion rates, and low-concentration of intermediate products [42,43]. Upham et al. developed a conceptual process model and evaluated the techno-economic feasibility of molten-metal methane pyrolysis [44]. They proposed the use molten Fe as the heat transfer medium, and found the cost of H_2 to be comparable to SMR-based H_2 production. Gregory et al. conducted an optimization-based techno-economic analysis of an LMBR system to produce H_2 for an industrial boiler, and a petrochemical plant in California [45]. They reported that in locations with high emission prices, levellized cost of H_2 could be $0.39/kg$H_2$, much lower than the cost of hydrogen produced from SMR, which varies $1.5-$2/kgH_2. An industrial project to demonstrate molten-metal methane pyrolysis is being developed jointly by Wintershall and Karlsruhe University of technology in Germany [46].

3. Methodology

The techno-economic assessment framework, developed for assessing green chemical technologies at low technology readiness level (TRL) was used in this work [47]. Market demand and future projections were assessed in the first step. Conceptual process models, and material and energy balance models were developed to get preliminary estimates (30% accuracy) of the specific energy demand, emissions, and component sizes in the second step. This was followed by an economic analysis i.e. calculation of the NPV and IRR of the proposed production plants from an investor's perspective. The final step involved conducting a sensitivity and uncertainty analysis, with NPV and IRR as the target variables.

3.1. Market analysis and demand assessment

Steel demand is projected to increase by 30% in 2050 [4]. However, the market for low-carbon steel technologies is not well-established. The recent policy shift towards decarbonisation of all sectors of the economy, and emphasis on the use of climate-neutral industrial products could increase the demand for low-carbon steel in the future [48–50]. Steel demand has traditionally come from the infrastructure sector i.e. construction, shipping, power-generators etc. Achieving a zero-carbon footprint across the value chain is becoming an important strategic objective for different manufacturing industries i.e as the transport sector transitions from internal combustion engines based vehicles to battery electric vehicles, the demand for low-carbon steel to manufacture automotive body parts could increase. Similarly, electricity sector's transition from fossil fuel based power plants to wind and solar generators could lead to an increased demand for low-carbon steel. Iron and steel is used to build the wind tower structure, gearbox, generator and turbine transformers. The steel intensity of existing wind turbine models varies from 107 to 132 t/MW of installed capacity [51]. Solar photovoltaic (PV) plants require 67.9 t/MW of steel [51]. According to estimates by the international renewable energy agency (IRENA), 6 Terawatt (TW) of wind and 9 TW of solar generators should be installed by 2050, increasing the share of renewable electricity generation to 61% from the current 10% to limit the harmful impacts of anthropogenic climate change [52]. This target could translate into a huge demand for low-carbon steel.

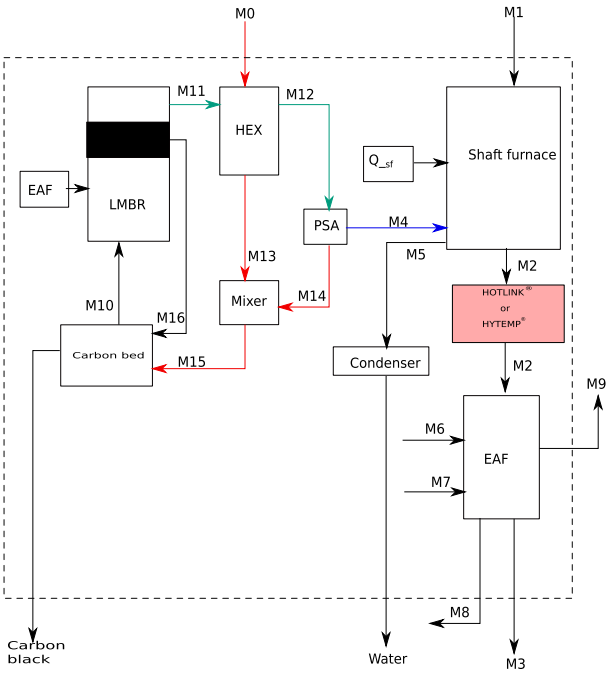

(a) Scenario 1 : H_2-SF-EAF system, H_2 is produced in a liquid metal bubble column reactor(LMBR), through methane pyrolysis. The heat is supplied by an EAF.

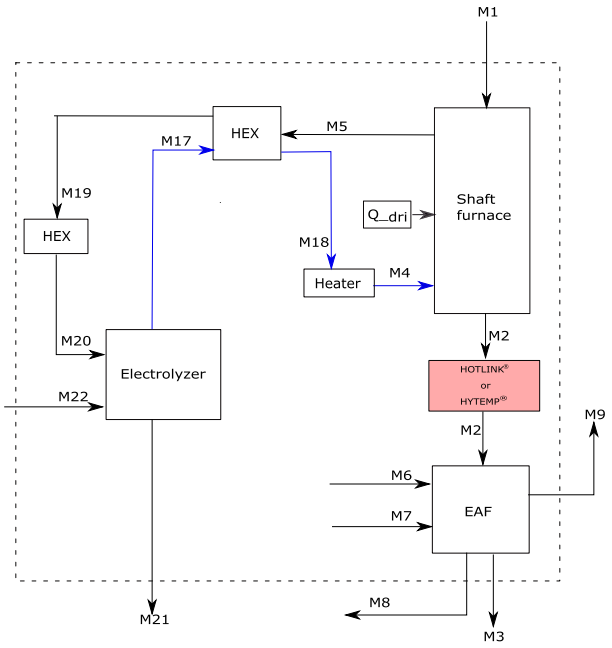

(b) Scenario 2: H_2-SF-EAF system, H_2 is produced by water electrolysis in a low-temperature alkaline electrolyser.

Fig. 1. (a) Scenario 1 : H_2-SF-EAF system, H_2 is produced in a liquid metal bubble column reactor(LMBR), through methane pyrolysis. The heat is supplied by an EAF. (b) Scenario 2: H_2-SF-EAF system, H_2 is produced by water electrolysis in a low-temperature alkaline electrolyser.

3.2. *Conceptual process modelling*

Conceptual process models were developed for both scenarios to calculate the material and energy balances. Calculations are based on the production of one ton of liquid steel under steady state conditions. Integrated material and energy balance calculations were performed across the control volumes of major components of the proposed systems. The process schematics of the systems considered in scenario 1 and scenario 2, used for developing the models are presented in Fig. 1a and Fig. 1b respectively. The steel production process can be divided into three sub-processes i.e. production of reducing agent (hydrogen), iron production in the shaft furnace, and conversion of iron to steel in the

Table 1
The reactor dimensions (M), temperature (°C), pressure, conversion factors (%), methane feed rate (kg/s) have been taken from [65]

Length	Diameter	Volume(Tin)	Temperature	Pressure	Conversion factor	CH_4 feed	H_2 flow
m	m	Tons	K	Bar	percentage	kg/hr	ton/hr
8.66	5.21	850	1443	19	0.90	29.39	24.03

EAF. The conceptual process flow diagram for the iron and steel production process using a shaft furnace and an EAF, is similar to the ones proposed by [30,17,5]. The difference in the overall material and energy balance of the two systems is attributed to the hydrogen production subprocess. Material flow through the components was evaluated using stoichiometric values of the reactants and products. It is assumed that the reactions reach completion in a single-pass, unless it is stated otherwise. The specific heat and enthalpy of the different species were calculated using the Shomate equation, as described in Eqs. (1) and (2). The coefficients of the Shomate equations were taken from NIST webBook [53].

$$C_p^{\circ} = A + B^*t + D^*t^2 + D^*t^3 + E/t^2 \tag{1}$$

$$H^{\circ} - H^{\circ}_{298.15} = A^*t + B^*t^2/2 + D^*t^3/3 + D^*t^4/4 - E/t + F - H \tag{2}$$

3.2.1. Iron production in the shaft furnace

The shaft furnace is a counter current flow reactor [54]. The iron ore pellet enter the shaft furnace from the top, through the stream **M1** at ambient temperature. Impurities have an adverse impact on the reaction kinetics, and should be limited to less than 5% [55]. The impurities are primarily composed of Al_2O_3 and SiO_2. The iron ore pellets react with the hydrogen gas, which enters the shaft furnace from the bottom of the furnace at 1173 K, represented by **M4**. The reduction of iron oxide to metallic iron occurs in three steps, where hematite (Fe_2O_3) is reduced to magnetite(Fe_3O_4), followed by magnetite's reduction to wustite (FeO), and subsequently to metallic Fe. The reduction steps are presented in the Eqs. (3)–(5). The heat of the reaction under standard conditions is 99.5 kJ/mol [56].

$$3Fe_2O_3(s) + H_2(g) \rightarrow 2Fe_3O_4(s) + H_2O(g) \tag{3}$$

$$Fe_3O_4(s) + H_2(g) \rightarrow 3FeO(s) + H_2O(g) \tag{4}$$

$$FeO(s) + H_2(g) \rightarrow Fe(s) + H_2O(g) \tag{5}$$

The reduction of Fe_2O_3 by H_2 is a non-catalytic, heterogeneous solid–gas endothermic reaction, where the overall reaction rate is dependent on the heat and mass transfer phenomena, and the rate of chemical reaction [57]. At higher temperatures, the chemical reaction rate increases exponentially, and diffusion of hydrogen through the laminar layer of hematite pellet is the rate limiting step [58]. Detailed analysis of the parameters affecting the overall reaction kinetics can be found in the literature [59,57,58,60].

Metallization rate of 94% is achieved in the H_2-SF [59]. The reduced iron exits the shaft furnace through stream **M2**, which is composed of metallic iron, wustite and impurities. The stream **M2** could be charged to the EAF at 873 K through the HOTLINK® or HYTEMP® process developed by MIDREX and ENERGIRON technologies respectively [61,62]. Energy consumed for the transfer of hot-metal to the EAF has not been considered in the present model. Although it's difficult to implement a hot-metal transport system in an existing steel plant, arrangements for gravity based transfer of hot-metal could be included in the design phase of a greenfield plant. The unreacted hydrogen, and steam produced as a by-product of the reduction reaction exit the reactor through the exhaust stream, **M5**, at 573 K [31]. A condenser is used to separate hydrogen, and water from the exhaust stream. Electrical resistance heaters are used to supply thermal energy to the shaft furnace.

3.2.2. Steel production in an EAF

The EAF is charged with 100% hot-DRI, and is heated to 1923 K. It exits the EAF, through the stream **M3**. The value of **M3** is fixed to one ton. Carbon fines of biogenic origin are added to the EAF through the stream **M6**. Carbon is required for the conversion of iron to steel, reduction of wustite to iron, and for the formation of CO. CO promotes froth formation, which is crucial for effective slag removal. The presence of CO gas improves the overall heat transfer rate from the graphite electrodes to the melt. It is assumed that 20 kg/tls of carbon is added [63]. Slag formers, **M7**, (mixture of CaO and MgO) are added to remove impurities, and to increase the life of the refractory lining of the furnace [64]. The slag exits the EAF through **M8**. The exhaust gases, composed primarily of CO_2,O_2 and N_2, exit the EAF through stream **M9** at 1773 K. Assumptions related to the air -infiltration, graphite electrode consumption etc. were taken from the literature [63].

Thermal energy is supplied by the electric arc formed between the graphite electrodes, and exothermic oxidation reactions. The reduction reactions of FeO and C, and the reaction between carbon and O_2 have been considered in the present model. The reactions are presented in Eqs. (6)–(8) respectively. An electrical efficiency of 0.85 has been considered for the EAF to account for losses from the transformer, rectifier, electrodes, radiative and convective heat transfer etc. Kirschen et al. presented a similar approach to calculate the energy consumption of an EAF [64].

$$FeO(s) + C(s) \rightarrow Fe(s) + CO(g) \tag{6}$$

$$2C(s) + O_2(g) \rightarrow 2CO(g) \tag{7}$$

$$C(s) + O_2(g) \rightarrow CO_2(g) \tag{8}$$

3.2.3. Scenario 1: LMBR subsystem

Catalan et al. designed an LMBR system for the production of 200 kta^{-1} using a coupled hydrodynamic and kinetic model [65]. Molten tin was used as the heat transfer medium in the LMBR and ten different configurations of the LMBR were presented by the authors. Configuration with the highest conversion factor, and smallest volume was evaluated in this model. The mass flow rates of H_2, CH_4, solid-carbon were converted to the mass flows per ton of liquid steel (kg/tls). LMBR dimensions and operational parameters are presented in Table 1. Thermodynamic properties of liquid tin were calculated using correlation provided by [66], and are presented in Eq. (9). The correlation is valid in the temperature range of $800 \leqslant T \leqslant 3000K$. The density of liquid tin was calculated using Eq. (10) [67].

$$\Delta H = -1285.372 + 28.4512^*T \tag{9}$$

$$\rho_{tin} = C_3 - C_4(T - T_{ref}) \tag{10}$$

Where $C_3 = 6979\ kgm^{-3}$,$C_4 = 0.652\ kgm^{-3}\ K^{-1}$, and $T_{ref} = 505.08$ K is the melting point of tin. Eq. (10) is valid in the temperature range of $506 \leqslant T \leqslant 1950$ K.

Natural gas (100% CH_4) enters the system through the stream **M0**, at high pressure and ambient temperature. It is pre-heated in the heat recovery heat exchanger (HEX) by the stream **M11**, which is a mixture of H_2 and unreacted CH_4 exiting the LMBR at 1443 K. The stream **M11** exits the heat exchanger as **M12** at 1173 K. CH_4 is separated in the pressure swing adsorber(PSA), and exits as stream **M14**. The stream **M13** and **M14** are mixed and enter the carbon-bed at an elevated temperature, through the stream **M15**. The carbon-bed can be visualized as a

solid–gas tubular heat exchanger [44]. The stream **M15** is heated to 973 K by the incoming stream of solid-carbon(**M16**). **M10**, enters the LMBR from the bottom, where a sparger disperses the pressurised gas into bubbles. Gas bubbles rise through the LMBR. They contain the solid-carbon particles, H_2, and CH_4 inside them, which are released at the top of the liquid tin surface. Molten metal acts as a heat transfer medium, providing heat for the endothermic decomposition of methane. The low-density carbon is insoluble in liquid tin, it can be readily removed in a continuous process in a manner similar to a floatation cell as is done routinely in slag removal. LMBR is made of 120 mm stainless steel, and is lined with a refractory layer of 600 mm, made of MgO bricks to sustain the high-temperatures inside the reactor [38]. An EAF is used for melting tin, and providing thermal energy to the LMBR [44].

3.2.4. Scenario 2: water electrolysis for hydrogen production

H_2 is produced using a low-temperature alkaline electrolsyer, consuming 50 KWh/kgH_2. The hydrogen stream, **M17** exiting the electrolyser is pre-heated in the heat recovery heat exchanger to **M18**. Heat is recovered from the shaft-furnace exhaust stream, **M5**, in the heat exchanger. An electrical heater is used to raise the temperature of the stream **M18** to the 1173 K. The shaft-furnace exhaust gases enter the condenser through the stream **M19**, lowering it's temperature from 393 K to 343 K. Purified condensed water enters the electrolyser through the stream **M20**. Additional water requirements are met through the stream **M22**, to account for losses in the circuit. O_2 is produced as a by-product of the water-electrolysis and exits the electrolyser through the stream **M21**.

3.3. Economic evaluation

Preliminary sizing of the main process equipment (reactors, pressure vessels, EAF) was done for a 3.35 Mta^{-1}) steel production plant, which is comparable to the size of NG-reformer based DRI-EAF plants in operation [68]. H_2 production capacity of 200 kta^{-1} was considered in both scenarios. Preliminary costs of the main process equipment were converted to the total capital costs using Lang factors from Sinnot [69]. The H_2-SF-EAF system plants were modelled as first-of-its-kind plants. A Lang-factor of five was considered for the H_2-SF-EAF system system, while a Lang factor of ten was used for the LMBR based hydrogen production system. The operational costs are comprised of the cost of iron ore, electricity, natural gas, and shaft furnace and EAF operational costs. A fixed price of electricity has been used to calculate the financial parameters for the plant. Only the direct emissions from the plants were used to evaluate the annual emissions cost. The annual maintenance cost was considered to be 2% of the capital cost, and a labour cost of 20$/tls was considered in the model [69]. The levellized cost of production (LCOP) was calculated for both scenarios by considering the annualized capital, operational, labour, maintenance, and emission costs of the system, using Eqs. (11) and (12).

$$LCOP = \frac{C_{capex}{}^{*}ACC + C_{opex} + C_{maint} + C_{labour} + C_{emission}}{Annual\,steel\,production} \tag{11}$$

$$ACC = \frac{r^{*}(1+r)^{n}}{(1+r)^{n}-1} \tag{12}$$

A discounted cash flow analysis was conducted to compare the NPV and IRR of the investment. NPV was calculated using Eq. (13). IRR is calculated as the discount rate at which the NPV of the cash flow is zero. The salvage value of the equipment after the end of plant life was assumed to be zero, and a linear depreciation rate has been considered. A tax rate of 25% was assumed for the calculations.

$$NPV = \sum_{n=1}^{n} \frac{CF}{(1+r)^{n}} \tag{13}$$

Where, ACC, CF, r, and n refer to the annuity factor, cumulative cash flow, discount rate, and the project life respectively. The economical parameters used for the calculations are presented in Table 2.

Table 2
Economical parameters considered for the H_2-SF-EAF system system.

Plant life	Plant construction	Discount rate	Tax rate	Depreciation	Steel output	H_2 output
Years	Years	%	%	N.A	Mt/year	Kt/year
20	2	8	25	linear	3.07	200

Table 3
Assumptions used in the techno-economic assessment model.

Capital cost assumptions			
Equipment	Cost ($)	Lifetime	Reference/remark
Electrolyser (Million $/MW H_2)	0.704	90000 h	[70]
Stack replacement (Million $/MW H_2)	0.540	100000 h	[70]
Shaft furnace ($\$t^{-1}$DRI/year)	240	20 years	[31]
Electric arc furnace ($\$t^{-1}$ steel/year)	140	20 years	[31]
Operational cost assumptions			
Item	Cost	Unit	Reference/remark
Iron ore	90	$/t	[71]
Electricity	56	$/MWh	[72]
Natural gas	6.58	$/MMBTU	[72]
DRI OPEX	12	$/tls	[73]
EAF OPEX	33	$/tls	[73]
CO_2 emission	35	$/t$CO_2$	[74]
Revenue stream assumptions			
Product	Price	Unit	Reference/remark
Carbon steel	700	$/t	[71]
Carbon	200	$/t	[44]
Oxygen	40	$/t	Market price of O_2

Revenue is generated from the sale of steel and by-products. Solid-carbon and oxygen are produced as a by-products of methane pyrolysis and water electrolysis respectively. Both by-products could be sold to generate additional revenue. Solid-carbon produced during methane pyrolysis is used in the manufacturing industries i.e. automobile tires, graphite electrodes, printer ink pigments, graphite electrodes etc. [27]. O_2 has many industrial applications. Assumptions related to the costs, and revenue used in the model are presented in Table 3.

3.4. Sensitivity and uncertainty analysis

There are different sources of uncertainty in the model inputs. They arise from the fluctuations in the price of internationally traded commodities (iron ore, natural gas, carbon price etc.), and price of input parameters such as electricity cost, emission costs. The technologies analyzed in this work are at low TRL, hence values of input parameters such as electrolyser efficiency and cost are uncertain. Local and global sensitivity analysis were conducted to apportion the uncertainty in the model output to different model inputs [75]. The NPV and IRR of the system were selected as the target variables. In the first step a local parametric sensitivity analysis was conducted [76]. The input parameters (uncertain factors) were varied by ±20% from their base values, and percentage change in the output values were evaluated.

A global sensitivity analysis was conducted using the sobol sensitivity indices approach to ascertain the uncertainty of the NPV and IRR values, based on the global uncertainty in the input parameter values [77]. Sobol sensitivity analysis determines the contribution of each input parameter, and their interactions to the overall model output

Table 4
Lower and upper bounds of input parameters used for the global sensitivity analysis.

Target Parameters: NPV and IRR			
Parameter	Lower bound	Upper bound	Unit
Tax rate	25	35	Percentage
Interest rate	0.06	0.12	Percentage
Electricity price	20	60	USD/MWh
Natural gas price	4	10	USD/MMBTU
Iron ore cost	75	120	USD/ton
Emission cost	35	200	Euro/tCO_2
Carbon steel price	600	700	USD/ton
Carbon price	100	300	USD/ton
Electrolyser efficiency	45	60	KWh/kgH_2
Electrolyser capital cost	0.2	0.7	Million \$/MWH_2

variance. The global sensitivity analysis was carried out using the SALib library to evaluate the Sobol first-order and Sobol total-order sensitivity indices [78]. The selected input parameters, and their lower and upper bounds are provided in Table 4.

4. Results

This section outlines the results of the techno-economic assessment. The material and energy balance, specific energy consumption, emissions, economic parameters, and results of the local and global sensitivity analysis are presented.

4.1. Material and energy balance

The material and energy flows through the different components of the steel production systems in presented in Table 5. It has been divided into three sub-processes as described in Section 3.2. The streams **M1** to **M9** represent the iron and steel production sub-process. Material and energy flows through the LMBR based H_2 production sub-system are presented by the streams **M0**, and **M10** to **M16**. The streams **M17** to **M22** depict the material and energy flows through the electrolyser based hydrogen production subsystem.

Approximately 59 kg of H_2 is required for the reduction of 1.5 ton of iron ore, required for one ton of steel production, considering a metallization rate of 94%, and impurity content of 5% in the iron ore pellets. Stoichiometric requirement of H_2 for iron oxide reduction is 54 kg/tls (considering 100% conversion of FeO in the EAF). A higher quantity of H_2 is considered in this model to account for 10% losses, owing to leakage, dissolution in water and other solid streams. The H_2 requirement is similar to the ones reported in the literature [31,30,25,5]. For the methane pyrolysis based system 261.6 kg of CH_4 is required, resulting in the production of 178 kg of solid-carbon as a by-product. In the electrolyser based system, the stream **M18** is heated to the shaft furnace temperature of 1173 K.

4.2. Specific energy consumption

Both systems were assumed to be connected to the electricity grid, and all energy requirements of the plants (except CH_4 used in the LMBR) were met by grid-electricity. The SF and the EAF have a combined electricity consumption of 0.79 MWh/tls. The endothermic reduction of Fe_2O_3 in the shaft furnace results in an additional electrical energy demand of 0.252 MWh/tls ($\eta = 0.85$). The EAF uses 0.537 MWh/tls ($\eta = 0.8$) of electricity. The total electricity requirements are higher than the NG-reformer based DRI-EAF unit, which requires approximately 0.680 MWh/tls. Thermal energy demand in the NG-reformer based DRI units is met by the exothermic reaction between CO and Fe_2O_3.

In scenario one, the SEC was found to be 5.16 MWh/tls. CH_4 entering the reactor is pre-heated to 973 K by exchanging heat with the streams **M11**, **M16** and **M14**. 55% of the thermal energy contained in the solid-carbon stream, **M16**, is recovered. The LMBR consumes 0.71 MWh/tls of electricity at an EAF efficiency of 80 %, which is slightly higher than 0.51 MWh/tls ((reported as 31 MJ/kgH_2) calculated by Upham et al. for a similar system [44]. They considered 90% sensible heat recovery from the H_2 stream exiting the reactor and solid-carbon stream, along with an EAF efficiency of 90 % leading to slightly lower electricity consumption. In addition, CH_4 used in LMBR as a chemical feedstock, corresponds to

Table 5
Material and energy flows through the different components of the steel production systems, considering a metallization rate of 0.94 and an impurity content of 5% in the iron ore pellets. Reaction enthalpy values are not presented in this table. More details about the calculations can be found in the Jupyter notebooks [79].

Stream	Description	Mass flow in kg/tls	Temperature in K	Enthalpy in KWh/tls
	Shaft furnace-Electric arc furnace subsystem			
M1	Fe_2O_3 pellets and impurities	1527.91	298	0.00
M2	Fe, FeO, and impurities	1089.48	873	99.02
M3	Liquid steel	1000.00	1923	324.84
M4	H_2 stream (reducing gas)	59.25	1173	211.99
M5	Shaft furnace exhaust	489.31	573	76.65
M6	Carbon fines	20.00	298	0.00
M7	Slag formers	50	298	0.00
M8	EAF slag stream	126.39	1923	75.07
M9	EAF exhaust stream	230.00	1173	105.22
M_{air}	Infiltrated air	250.00	298	0.00
	Liquid metal bubble column reactor subsystem			
M0	Natural gas from pipeline	263.37	298	0.00
M10	Pre-heated methane	263.37	973	166.07
M11	H_2 and CH_4 at LMBR outlet	85.38	1443	316.48
M12	H_2 and CH_4 from HEX	85.38	1173	235.20
M13	Pre-heated incoming CH_4 stream	263.37	585	83.96
M14	CH_4 stream from PSA	26.12	1173	23.17
M15	Mixed CH_4 stream	263.37	616	96.33
M16	Carbon stream from LMBR	177.77	1443	100.37
	Electrolysis subsystem			
M17	H_2 from electrolyser	59.56	343	1.12
M18	Heated H_2	59.56	448	31.85
M19	H_2O after HEX	486.82	393	25.47
M20	Condensed H_2O	481.43	343	85.85
M21	O_2 from electrolyser	476.49	343	6.63
M22	H_2O for electrolysis	52	298	0.0

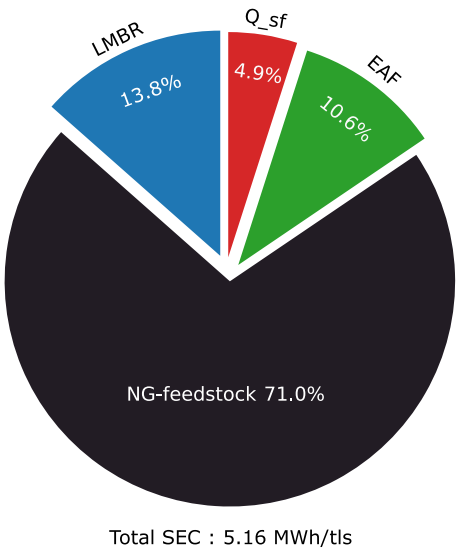

(a) Energy consumption of the methane pyrolysis based H_2-SF-EAF system system

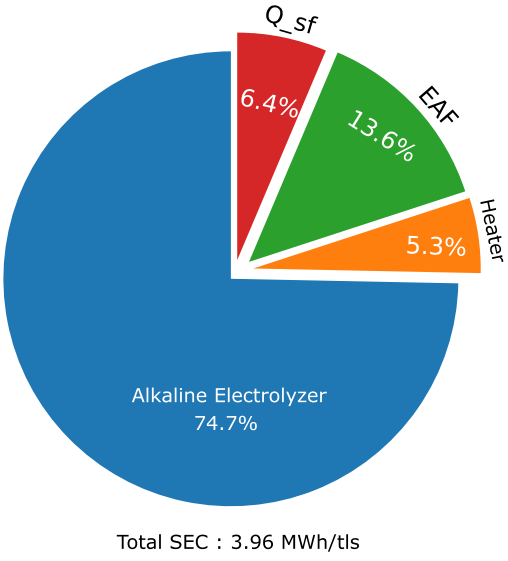

(b) Energy consumption of the electrolyser based H_2-SF-EAF system system

Fig. 2. (a) Energy consumption of the methane pyrolysis based H_2-SF-EAF system system. (b) Energy consumption of the electrolyser based H_2-SF-EAF system system.

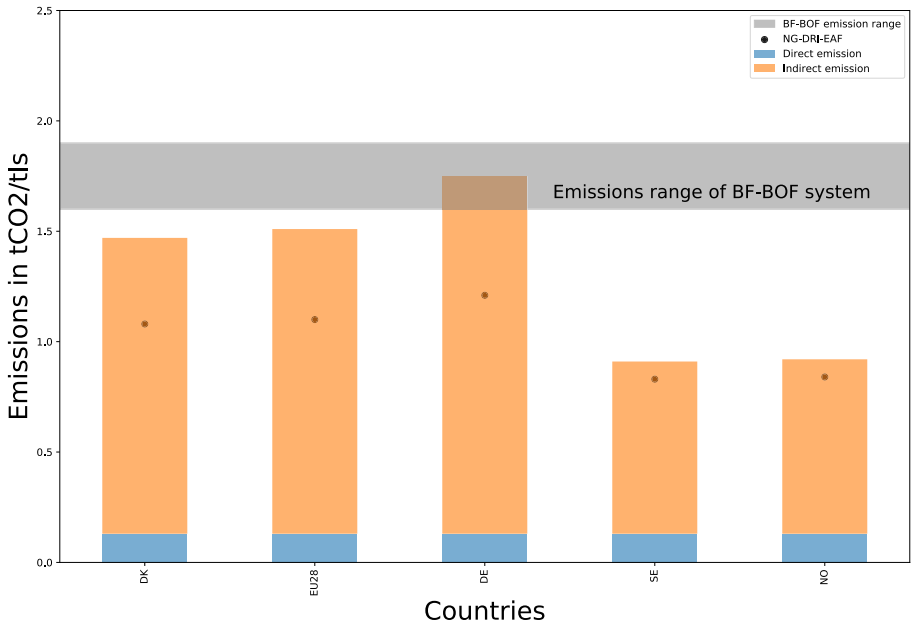

(a)

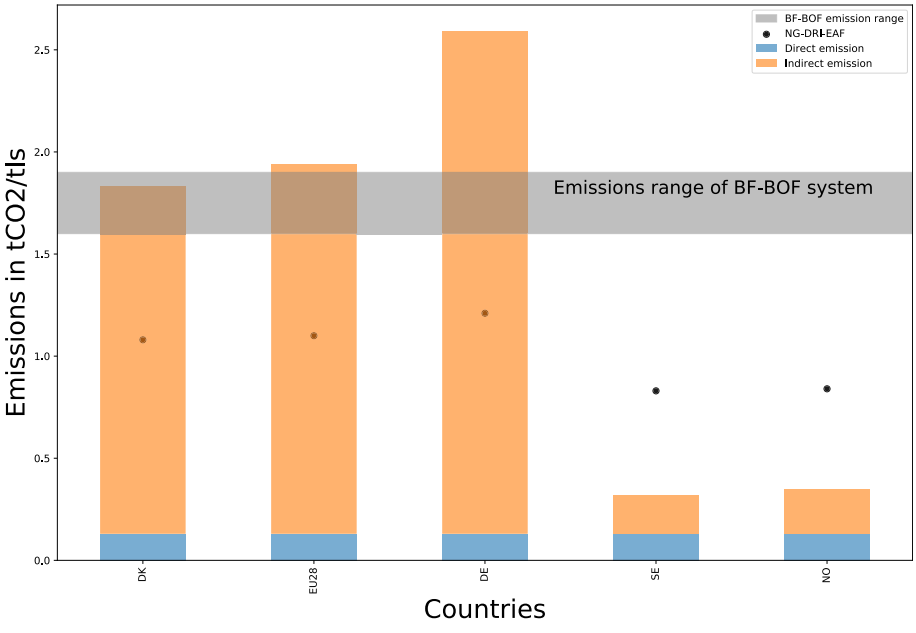

(b)

Fig. 3. (a) Direct and indirect emissions from the methane pyrolysis based H_2-SF-EAF system. (b) Direct and indirect emissions from the electrolysis based H_2-SF-EAF system. The grey band on the top of chart depicts the range of emissions from BF-BOF based steel production. The black dots represent the total emissions a NG-reformer based DRI-EAF system.

an energy consumption of 3.65 MWh/tls at lower heating value of 48 MJ/kg of CH_4. The SEC of a NG-reformer based DRI-EAF system is much lower at 3.26 MWh/tls [16].

The water electrolysis based H_2-SF-EAF system system has an SEC of 3.96 MWh/tls, at an electrolyser efficiency of 50 KWh/kgH_2. Electrolysers consume 2.96 MWh/tls or 74.7% of the total electricity. The H_2stream, exiting the electrolyser is pre-heated by exchanging heat with the SF exhaust gases. It exits the heat exchanger at a 448 K. The H_2 stream is subsequently heated to the reactor temperature of 1173 K °C in an electrical heater consuming 0.211 MWh/tls of electricity ($\eta = 0.85$. In the literature, the SEC value of comparable systems vary from 3.48 MWh/tls [30,17] to 3.95 MWh/tls [31]. The difference in the SEC's originate from the use of different values of electrolyser efficiency (depends on the projected installation year of the plant), use of scrap in the EAF, thermal energy requirements of the shaft-furnace, purge-gas requirements etc. The energy consumption of the different components for both scenarios is depicted in Fig. 2a, and Fig. 2.

4.3. Emissions

4.3.1. Direct emissions

Direct emissions of 129.4 kgCO_2/tls have been considered for both scenarios, which are related to CO_2 emissions from the EAF. The EAF emissions originate from the use of carbon fines, graphite electrodes and

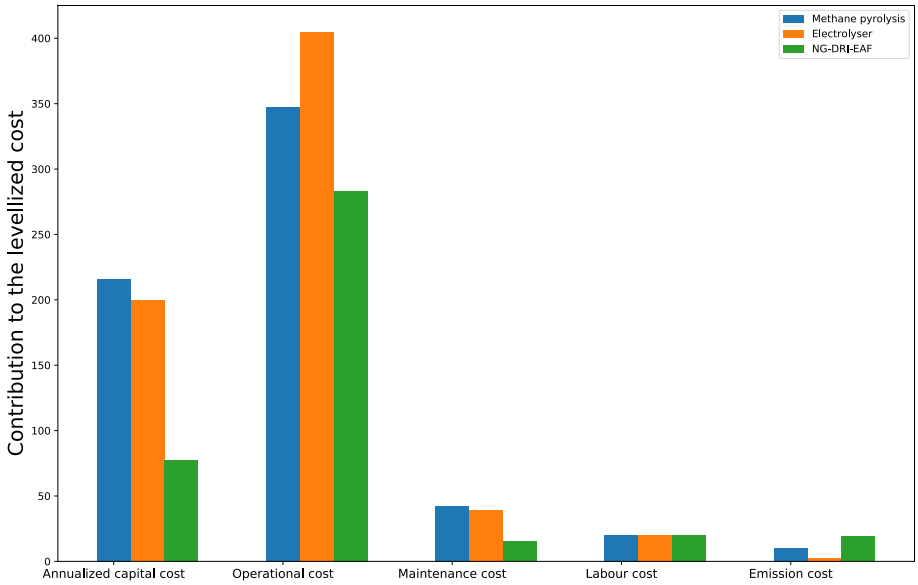

Fig. 4. Breakup of levellized cost of production of steel for both scenarios. The costs are compared with an NG reformer based DRI-EAF based system, operating under similar conditions.

the production of lime.

4.3.2. Indirect emissions

The indirect emissions are related to the use of electricity and natural gas. The pellet making process accounts for the release of 120 $kgCO_2$/tls of emissions. In the HYBRIT project, new production methods are being developed to decarbonise the pellet making process [17]. An upstream emission of 17 gCO_2/MJ has been considered for natural gas, taking into account the fugitive emissions caused by production, transport and distribution of natural gas [80]. Indirect emissions associated with electricity use are dependent on the electricity mix of the region, and is represented by the grid emission factor (GEF) [81].

4.3.3. Total emissions

The total emissions were calculated as the sum of the direct and indirect emissions. Considering a GEF of 412 $kgCO_2$/MWh, corresponding to the GEF of EU-28 [81]. The total emissions in scenario one were 0.90 tCO_2/tls. The value is comparable to the emissions of 0.98 tCO_2/tls from a reforming based NG-DRI-EAF system. More natural gas is consumed in the LMBR, for the production of reducing agent (H_2) resulting in a higher amount of indirect upstream emissions. The impact of variation in the GEF on emissions for LMBR system is depicted in Fig. 3a.

The total emissions from the electrolyser based H_2-SF-EAF system system were found to be 1.93 tCO_2/tls. In countries with cleaner electricity mix, the total emissions for electrolyser based H_2-SF-EAF system system were found to be much lower than NG-reformer based DRI-EAF systems. If electricity is supplied from renewable energy generators, the total emissions in the second scenario could be much lower, as can be seen in Fig. 3b from the lower emissions in Norway and Sweden.

4.4. Economic analysis

The methane pyrolysis based system has a lower LCOP of 631 $/t, compared to the LCOP of 669 $/t for the electrolyser based H_2-SF-EAF system. The LCOP value is at the higher end of values reported in the literature, as we have considered first-of-its kind plants, resulting in higher capital costs [30,31]. Additionally, we have considered maintenance, labour and emission costs in LCOP calculations, which were not included in the previous studies. The NG reformer based DRI-EAF system has a much lower LCOP of 414 $/t. The break-up of the LCOP is presented in Fig. 4. The annual operational costs contribute to more than 50% of the production costs in all three scenarios. Annualized capital costs have a significant contribution to the LCOP of methane pyrolysis based system. Compared to the low-carbon steel production routes, emission costs have the highest impact on the production costs of the NG reformer based DRI-EAF system. In a carbon constrained world, rising emission prices could increase production costs significantly for the NG reformer based DRI-EAF systems.

4.5. Discounted cash flow analysis

A discounted cash flow analysis was conducted for both the scenarios, under the economical assumptions presented in Table 2 and Table 3. The NPV was $1.07 billion for the first scenario, and $-5 million in the second scenario. At 10.01 %, the IRR of the methane pyrolysis based steelmaking unit was higher than the discount rate of 8%. The IRR of the electrolyser based H_2-SF-EAF system based steelmaking unit was found to be 7.98 %. A NG reformer based DRI-EAF system operating under the same conditions was found to have an NPV of $5.9 billion, and an IRR of 33.1%.

4.5.1. Local sensitivity analysis

The results of the local sensitivity analysis reveal that the NPV of the methane pyrolysis based H_2-SF-EAF system system are highly sensitive to changes in the carbon steel price and discount rate. The IRR of the system is sensitive to the carbon steel price, and the iron ore costs. The other significant factors are the electricity prices, and the natural gas price. The NPV and IRR of the electrolyser based H_2-SF-EAF system system are sensitive to changes in the carbon steel price, electricity cost, and the electrolyser efficiency. The results of the sensitivity analysis are presented in Fig. 5a, 5b, 6a, and 6b.

4.5.2. Global sensitivity analysis

The results of the global sensitivity analysis in the form of first order Sobol indices, and total order Sobol indices are presented in Fig. 7a and Fig. 7b. The values of the second order Sobol indices were found to be insignificant, indicating weak interaction between the input variables. It can be inferred that the interest rate, and carbon steel price have maximum contribution to the variance of methane pyrolysis system's NPV. The variance in the IRR value of the methane pyrolysis system stems from the uncertainty in carbon steel price, electricity price, and the cost of emissions. Variations in electricity cost, and carbon steel price

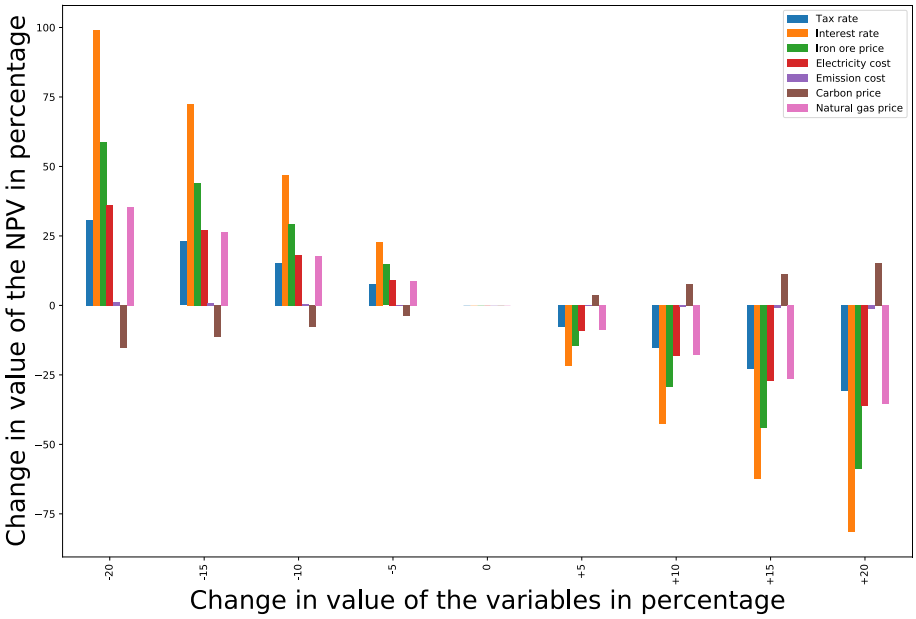

(a)

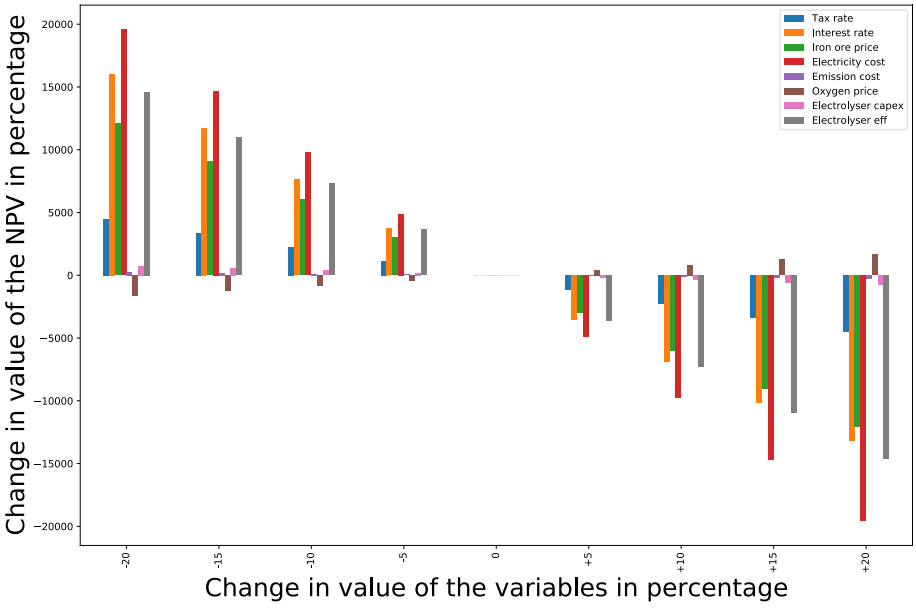

(b)

Fig. 5. The sensitivity of different parameters with NPV (a) Scenario one (b) Scenario two.

can be attributed with the maximum contribution to the variance in the NPV and IRR values of the electrolyser based system.

5. Discussion

Economic feasibility of the LMBR system is highly sensitive to the discount rate, owing to the higher capital costs of the system. The total capital cost of the methane pyrolysis based system was found to be $7.1 billion. LMBR system capex was $743 million and the H_2-SF-EAF system had a capex of $6.4 billion. Capital costs of the H_2-SF-EAF system steelmaking unit could reduce in the future as new plants are installed. The use of EAF for heating the LMBR has a major contribution to the LMBR capital costs. Tank-lined electric resistive heating elements made of silicon carbide could heat the reactor and lead to reduction in LMBR system costs [45]. The capital costs of the LMBR could be reduced by using a cheaper heat-transfer metal, or by using catalytic metals to lower the reaction temperature [82].

The operational costs of the electrolyser based system have the highest impact on the economic feasibility. The operational costs could be reduced by selecting regions with low electricity prices for installation of the plant. Improvements in the electrolyser efficiency could also reduce the operational costs. Using solid oxide electroysers (SOEC) for H_2 generation could reduce the electricity consumption, by utilizing heat from the shaft-furnace exhaust gases for steam generation [31]. Waste heat recovery from the EAF exhaust gases to heat the iron ore pellets could reduce the energy consumption, as they leave the EAF at 1773 K. Integration of renewable generators, with optimally sized electrolysers, and H_2 storage could allow the use of cheap renewable electricity for steelmaking [83]. Additional revenue generated by providing demand-response services to the electricity grid could also

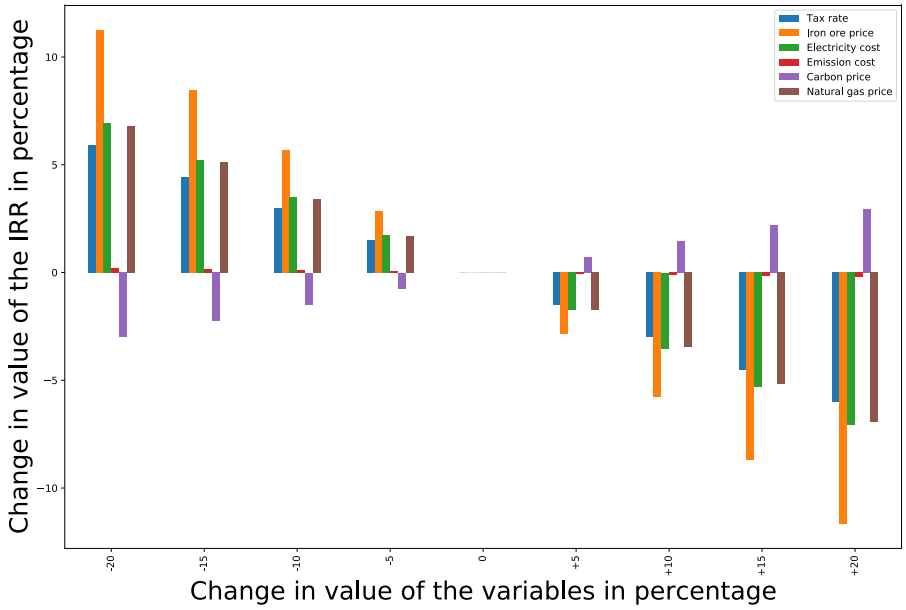

(a)

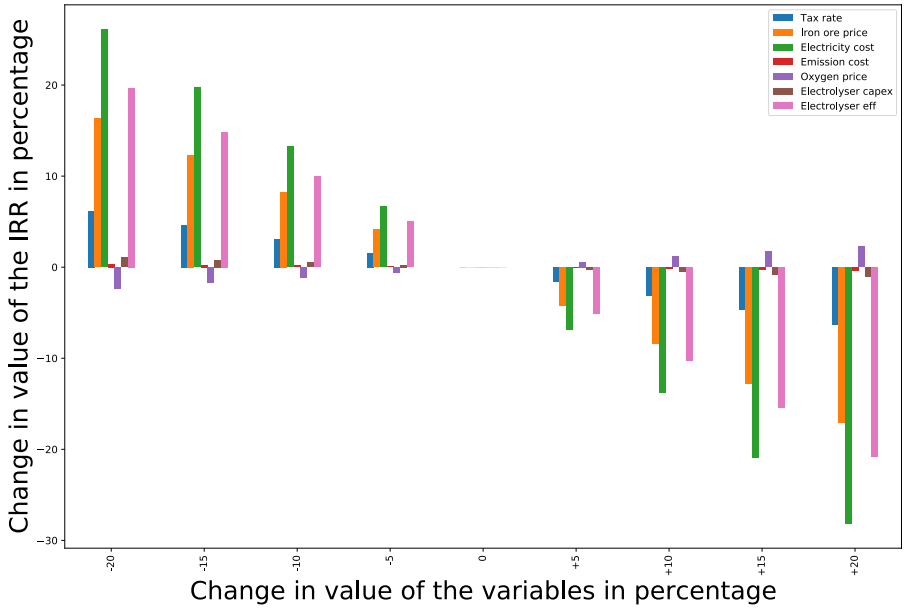

(b)

Fig. 6. The sensitivity of different parameters with IRR (a) Scenario one (b) Scenario two.

lower the cost of operation of the plants in the future by producing and storing large quantities of H_2 during times of low-electricity prices. However, availability of geological storage in close proximity to the steel production facilities is integral to leveraging the variations in the electricity prices as other storage alternatives are quite expensive.

6. Conclusion

A techno-economic assessment was conducted to evaluate the viability of integrating methane pyrolysis for H_2-SF-EAF system based low-carbon steel production. The assessment was conducted under two scenarios, and the results were compared. In the first scenario, hydrogen is produced by methane pyrolysis in a liquid metal bubble column reactor, and by low- temperature water electrolysis in the second scenario. The analysis was conducted from an investor's perspective for first-of-its-kind plants, leading to higher capital costs. In scenario one, the specific energy consumption was 5.15 MWh/tls, comprising of 1.37 MWh/tls of electricity, and 3.65 MWh/tls of natural gas consumption. In scenario two, 3.96 MWh/tls of electricity was consumed. The direct emission in both cases were found to be 128 kg/tls. Total emissions for electrolyser based steel production were found to be lower in regions with a cleaner electricity mix. The levellized costs of production were found to be $659 and $651 respectively, which are higher than the production costs from a reformer based NG-DRI-EAF system. The main results of the techno-economic assessment are presented in Table 6.

Integrating methane pyrolysis with an H_2-SF-EAF system system is techno-economically feasible and could play an important role in decarbonising steel production in the short and medium term. The authors recommend the development of a consortium of steel companies, natural gas companies, researchers, and universities to further develop

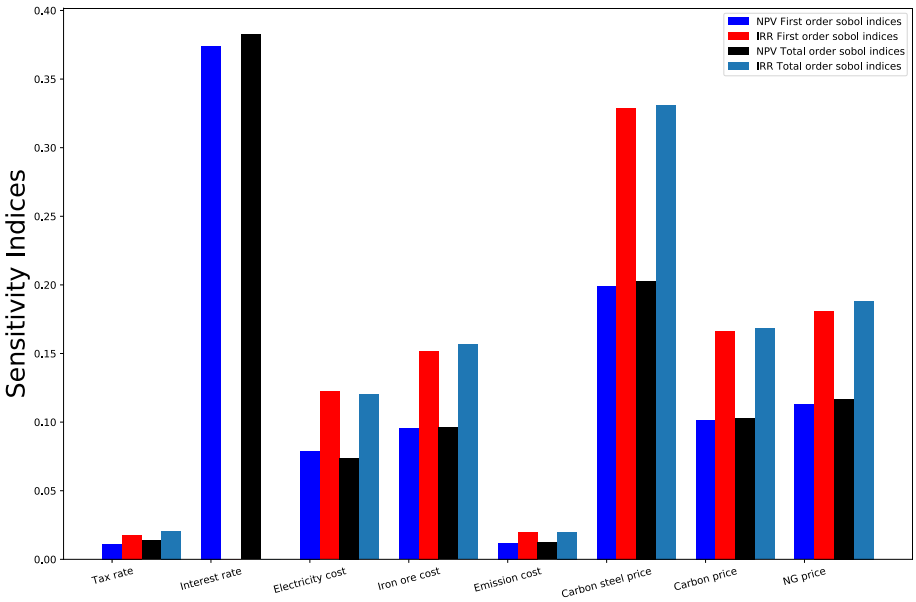

(a)

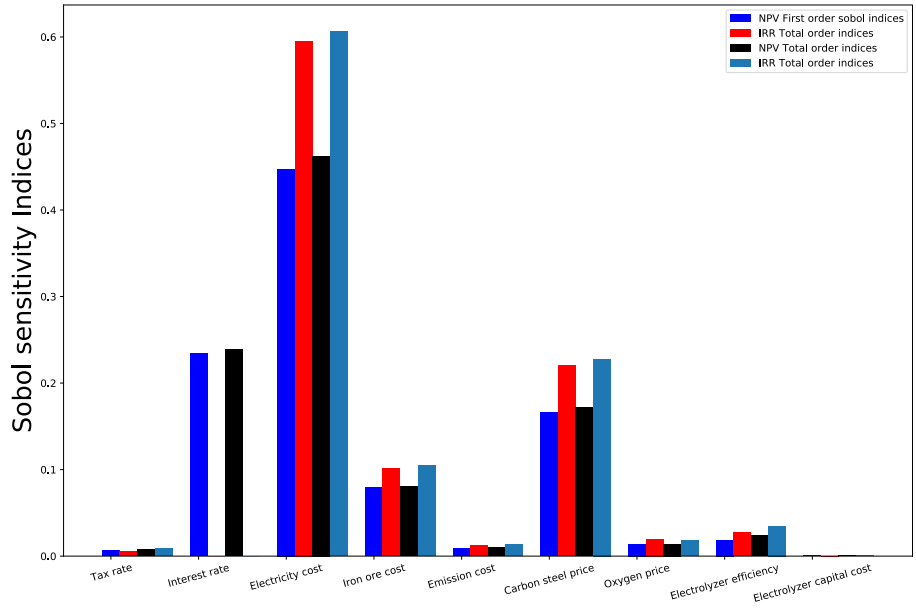

(b)

Fig. 7. (a) First order and total order Sobol indices calculated to quantify the uncertainty propagation in NPV and IRR values of the methane pyrolysis based H_2-SF-EAF system system. (b) First order and total order Sobol indices calculated to quantity the uncertainty propagation in NPV and IRR values of the water electrolyser based H_2-SF-EAF system system.

Table 6
Results from the techno-economic assessment analysis.

	SEC	Direct Emissions	CAPEX	OPEX	LCOP	NPV	IRR
Units	MWh/tls	$KgCO_2$/tls	$ Billion	$ Billion	$	$ Billion	%
LMBR-H_2-SF-EAF	5.16	129.42	7.15	1.17	631	1.07	10.09
Electrolyser-H_2-SF-EAF	3.96	129.42	6.6	1.38	669	−0.005	7.98
NG-DRI-EAF	3.26	541	2.56	0.95	414	5.9	33.1

the technology, especially in regions with access to cheap natural gas and clean grid electricity.

Data availability

The software codes developed for the analysis are hosted on Zenodo. The model is written in the Python programming language [79].

CRediT authorship contribution statement

Abhinav Bhaskar: Conceptualization, Methodology, Software, Writing - original draft, Visualization. **Mohsen Assadi:** Supervision, Validation. **Homam Nikpey Somehsaraei:** Supervision, Validation.

Declaration of Competing Interest

The authors declare that they have no known competing financial interests or personal relationships that could have appeared to influence the work reported in this paper.

Acknowledgement

This project has received funding from the European Union's Horizon 2020 research and innovation programme under the Marie Skłodowska-Curie grant agreement No 765515.

References

[1] IPCC. IPCC 2018: Summary for Policymakers. In: Global Warming of 1.5C. An IPCC Special Report on the impacts of global warming of 1.5C above pre-industrial levels and related global greenhouse gas emission pathways, in the context of strengthening the global, Tech. rep., IPCC; 2018.
[2] Flores-Granobles M, Saeys M. Minimizing CO_2 emissions with renewable energy: a comparative study of emerging technologies in the steel industry. Energy Environ Sci.https://doi.org/10.1039/d0ee00787k.
[3] M. Fischedick, J. Roy, A. Abdel-Aziz, A. Acquaye, J. M. Allwood, J.-p. Ceron, Y. Geng, H. Kheshgi, A. Lanza, D. Perczyk, L. Price, E. Santalla, C. Sheinbaum, K. Tanaka, Industry, Tech. rep., IPCC (2014).
[4] International Energy Agency. Iron and Steel Technology roadmap: Towards more sustainable steelmaking, Tech. rep., International energy agency; 2020. URL www.iea.org.
[5] Patisson F, Mirgaux O. Hydrogen ironmaking: how it works. Metals 2020;10(7):1–15. https://doi.org/10.3390/met10070922.
[6] Birat J-P. Society, Materials, and the Environment: The Case of Steel. Metals 2020;10(3):331. https://doi.org/10.3390/met10030331.
[7] Sarkar S, Bhattacharya R, Roy GG, Sen PK. Modeling MIDREX Based Process Configurations for Energy and Emission Analysis. Steel Research International, 89; 2018. p. 1700248. https://doi.org/10.1002/srin.201700248.
[8] Arens M, Worrell E, Eichhammer W, Hasanbeigi A, Zhang Q. Pathways to a low-carbon iron and steel industry in the medium-term – the case of Germany. J Clean Prod 2017;163:84–98. https://doi.org/10.1016/J.JCLEPRO.2015.12.097.
[9] Quader MA, Ahmed S, Ghazilla RAR, Ahmed S, Dahari M. A comprehensive review on energy efficient CO2 breakthrough technologies for sustainable green iron and steel manufacturing. Renew Sustain Energy Rev 2015;50(October):594–614. https://doi.org/10.1016/j.rser.2015.05.026.
[10] Fischedick M, Marzinkowski J, Winzer P, Weigel M. Techno-economic evaluation of innovative steel production technologies. J Clean Prod 2014;84(1):563–80. https://doi.org/10.1016/j.jclepro.2014.05.063.
[11] M. Weigel, M. Fischedick, J. Marzinkowski, P. Winzer, Multicriteria analysis of primary steelmaking technologies, Journal of Cleaner Production 112 (May 2013) (2016) 1064–1076. doi:10.1016/j.jclepro.2015.07.132.
[12] Toktarova A, Karlsson I, Rootzén J, Göransson L, Odenberger M, Johnsson F. Pathways for Low-Carbon Transition of the Steel Industry—A Swedish Case Study. Energies 13 (15).https://doi.org/10.3390/en13153840.
[13] Lopes DV, Ivanova YA, Kovalevsky AV, Sarabando AR, Frade JR, Quina MJ. Electrochemical reduction of hematite-based ceramics in alkaline medium: challenges in electrode design. Electrochim Acta 2019;327:135060. https://doi.org/10.1016/j.electacta.2019.135060.
[14] Nuber D, Eichberger H, Rollinger B. Circored fine ore direct reduction, Millenium steel 2006. URL http://millennium-steel.com/wp-content/uploads/articles/pdf/2006/pp37-40 MS06.pdf http://millennium-steel.com/wp-content/uploads/articles/pdf/2006/pp37-40 MS06.pdf.
[15] Elmquist H, Weber SA, Eichberger P. Operational results of the Circored fine ore direct reduction plant in Trinidad, STAHL UND EISEN (2002) 59–64 doi:0340-4803.
[16] Duarte P. Hydrogen-based steelmaking, Tech. rep., TenovaHYL; 2015. URLhttps://www.millennium-steel.com/wp-content/uploads/2019/05/MS2019-22-MS19-16.pdf.
[17] Pei M, Petäjäniemi M, Regnell A, Wijk O. Toward a fossil free future with hybrit: Development of iron and steelmaking technology in Sweden and Finland. Metals 2020;10(7):1–11. https://doi.org/10.3390/met10070972.
[18] Karakaya E, Nuur C, Assbring L. Potential transitions in the iron and steel industry in Sweden: Towards a hydrogen-based future? J Clean Prod 2018;195:651–63. https://doi.org/10.1016/j.jclepro.2018.05.142.
[19] Keys A, Van Hout M, Daniëls B. Decarbonisation options for the dutch steel industry. PBL Netherlands Environmental Assessment Agency 2019. Tech. Rep. november, URL www.pbl.nl/en.
[20] Langner LL, Arne, ArcelorMittal commissions Midrex to design demonstration plant for hydrogen steel production in Hamburg; 2019.https://corporate.arcelormittal.com/news-and-media/news/2019/sep/16-09-2019.
[21] Posdziech O, Schwarze K, Brabandt J. Efficient hydrogen production for industry and electricity storage via high-temperature electrolysis. Int J Hydrogen Energy 2019;4:19089–101. https://doi.org/10.1016/j.ijhydene.2018.05.169.
[22] Thyssenkrupp. World first in Duisburg as NRW economics minister Pinkwart launches tests at thyssenkrupp into blast furnace use of hydrogen; 2019.https://www.thyssenkrupp-steel.com/en/newsroom/press-releases/world-first-in-duisburg.html.
[23] ArcelorMittal. World first for steel: ArcelorMittal investigates the industrial use of pure hydrogen – ArcelorMittal; 2019. URLhttps://corporate.arcelormittal.com/news-and-media/news/2019/mar/28-03-2019.
[24] European Commission (EC), A hydrogen strategy for a climate-neutral Europe, Tech. rep., European commission, Brussels; 2020.
[25] Rechberger K, Spanlang A, Sasiain Conde A, Wolfmeir H, Harris C. Green Hydrogen-Based Direct Reduction for Low-Carbon Steelmaking, Steel Res Int 91 (11).https://doi.org/10.1002/srin.202000110.
[26] Whitmarsh L, Xenias D, Jones CR. Framing effects on public support for carbon capture and storage. Palgrave Commun 5(1).https://doi.org/10.1057/s41599-019-0217-x.
[27] Keipi T, Tolvanen H, Konttinen J. Economic analysis of hydrogen production by methane thermal decomposition: Comparison to competing technologies. Energy Convers Manage 2018;159(January):264–73. https://doi.org/10.1016/j.enconman.2017.12.063.
[28] Weger L, Abánades A, Butler T. Methane cracking as a bridge technology to the hydrogen economy. Int J Hydrogen Energy 2017;42(1):720–31. https://doi.org/10.1016/J.IJHYDENE.2016.11.029.
[29] Parkinson B, Balcombe P, Speirs JF, Hawkes AD, Hellgardt K. Levelized cost of CO_2 mitigation from hydrogen production routes. Energy Environ Sci 2019;12(1):19–40. https://doi.org/10.1039/c8ee02079e.
[30] Vogl V, Åhman M, Nilsson LJ. Assessment of hydrogen direct reduction for fossil-free steelmaking. J Clean Prod 2018;203:736–45. https://doi.org/10.1016/j.jclepro.2018.08.279.
[31] Krüger A, Andersson J, Grönkvist S, Cornell A. Integration of water electrolysis for fossil-free steel production. Int J Hydrogen Energyhttps://doi.org/10.1016/j.ijhydene.2020.08.116.
[32] Andersson J, Krüger A, Grönkvist S. Methanol as a carrier of hydrogen and carbon in fossil-free production of direct reduced iron. Energy Convers Manage: X 2020;7 (April):100051. https://doi.org/10.1016/j.ecmx.2020.100051.
[33] Wang IW, Kutteri DA, Gao B, Tian H, Hu J. Methane Pyrolysis for Carbon Nanotubes and COx -Free H2 over Transition-Metal Catalysts. Energy Fuels 2019;33(1):197–205. https://doi.org/10.1021/acs.energyfuels.8b03502.
[34] Monolith Materials, Monolith Materials: Olive Creek Plant; 2019. URLhttps://monolithmaterials.com/olive-creek/.
[35] M. Materials, Monolith plans carbon free ammonia plant.https://monolithmaterials.com/news/monolith-plans-carbon-free-ammonia-production-plant.
[36] Abbas HF, Wan Daud WMA. Hydrogen production by methane decomposition: a review. Int J Hydrogen Energy 2010;35(3):1160–90. https://doi.org/10.1016/j.ijhydene.2009.11.036.
[37] D. C. Upham, V. Agarwal, A. Khechfe, Z. R. Snodgrass, M. J. Gordon, H. Metiu, E. W. McFarland, Catalytic molten metals for the direct conversion of methane to

hydrogen and separable carbon, Science 358 (6365). doi:10.1126/science.aao5023.
[38] Parkinson B, Tabatabaei M, Upham DC, Ballinger B, Greig C, Smart S, McFarland E. Hydrogen production using methane: Techno-economics of decarbonizing fuels and chemicals. Int J Hydrogen Energy 2018;43(5):2540–55. https://doi.org/10.1016/j.ijhydene.2017.12.081.
[39] Abánades A, Rathnam RK, Geißler T, Heinzel A, Mehravaran K, Müller G, Plevan M, Rubbia C, Salmieri D, Stoppel L, Stückrad S, Weisenburger A, Wenninger H, Wetzel T. Development of methane decarbonisation based on liquid metal technology for CO2-free production of hydrogen. Int J Hydrogen Energy 2016;41(19):8159–67. https://doi.org/10.1016/j.ijhydene.2015.11.164.
[40] Palmer C, Tarazkar M, Kristoffersen HH, Gelinas J, Gordon MJ, McFarland EW, Metiu H. Methane Pyrolysis with a Molten Cu-Bi Alloy Catalyst, ACS Catal 9 (9). https://doi.org/10.1021/acscatal.9b01833.
[41] Serban M, Lewis MA, Marshall CL, Doctor RD. Hydrogen production by direct contact pyrolysis of natural gas. Energy Fuels 2003;17(3):705–13. https://doi.org/10.1021/ef020271q.
[42] Plevan M, Geißler T, Abánades A, Mehravaran K, Rathnam RK, Rubbia C, Salmieri D, Stoppel L, Stückrad S, Wetzel T. Thermal cracking of methane in a liquid metal bubble column reactor: experiments and kinetic analysis. Int J Hydrogen Energy 2015;40(25):8020–33. https://doi.org/10.1016/j.ijhydene.2015.04.062.
[43] Geißler T, Abánades A, Heinzel A, Mehravaran K, Müller G, Rathnam RK, Rubbia C, Salmieri D, Stoppel L, Stückrad S, Weisenburger A, Wenninger H, Wetzel T. Hydrogen production via methane pyrolysis in a liquid metal bubble column reactor with a packed bed. Chem Eng J 2016;299:192–200. https://doi.org/10.1016/j.cej.2016.04.066.
[44] Parkinson B, Matthews JW, McConnaughy TB, Upham DC, McFarland EW. Techno-economic analysis of methane pyrolysis in molten metals: decarbonizing natural gas. Chem Eng Technol 2017;40(6):1022–30. https://doi.org/10.1002/ceat.201600414.
[45] Von Wald GA, Masnadi MS, Upham DC, Brandt AR. Optimization-based technoeconomic analysis of molten-media methane pyrolysis for reducing industrial sector CO 2 emissions. Sustain Energy Fuels 2020;4(9):4598–613. https://doi.org/10.1039/D0SE00427H.
[46] U. MICHAELIS, Hydrogen from Natural Gas without CO2 Emissions; 2019. URL shorturl.at/jzBMS.
[47] Thomassen G, Van Dael M, Van Passel S, You F. How to assess the potential of emerging green technologies? Towards a prospective environmental and techno-economic assessment framework. Green Chem 2019;21(18):4868–86. https://doi.org/10.1039/c9gc02223f.
[48] E. Directorate-General for Internal Market, Industry, S. E. Commission), Masterplan for a competitive transformation of EU energy intensive industries enabling a climate-neutral, circular economy by 2050, Tech. rep., European commission; 2019.https://doi.org/10.2873/854920.
[49] Gielen D, Saygin D, Taibi E, Birat JP. Renewables-based decarbonization and relocation of iron and steel making: a case study. J Ind Ecol 2020;24(5):1113–25. https://doi.org/10.1111/jiec.12997.
[50] Rissman J, Bataille C, Masanet E, Aden N, Morrow WR, Zhou N, Elliott N, Dell R, Heeren N, Huckestein B, Cresko J, Miller SA, Roy J, Fennell P, Cremmins B, Koch Blank T, Hone D, Williams ED, de la Rue S, du Can B, Sisson M, Williams J, Katzenberger D, Burtraw G, Sethi H, Ping D, Danielson H, Lu T, Lorber J, Dinkel J Helseth. Technologies and policies to decarbonize global industry. Appl Energy 2020;266:114848. https://doi.org/10.1016/j.apenergy.2020.114848. Review and assessment of mitigation drivers through 2070.
[51] European Commission, Raw materials demand for wind and solar PV technologies in the transition towards a decarbonised energy system, Tech. rep., European commission; 2020.https://doi.org/10.2760/160859.
[52] IRENA. Global Renewables Outlook: Energy transformation 2050. Available at: https://www.irena.org/publications/2020/Apr/Global-Renewables-Outlook-2020, Tech. rep., International renewable energy agency; 2020.https://www.irena.org/publications/2020/Apr/Global-Renewables-Outlook-2020.
[53] Chase MW. NIST-JANAF thermochemical Tables, 4th ed., vol. 9, American Chemical Society; American institute of Physics for the National institute of standards and technology; 1998.
[54] Béchara R, Hamadeh H, Mirgaux O, Patisson F. Optimization of the iron ore direct reduction process through multiscale process modeling. Materials 2018;11(7):1094. https://doi.org/10.3390/ma11071094.
[55] Lu L, Pan J, Zhu D. Quality requirements of iron ore for iron production. In: Iron Ore, Elsevier; 2015. p. 475–504.https://doi.org/10.1016/B978-1-78242-156-6.00016-2.
[56] Wagner M. Thermal Analysis in Practice, Collected Applications Thermal Analysis.
[57] Spreitzer D, Schenk J. Reduction of iron oxides with hydrogen—a review. Steel Res Int 2019;90(10):1900108. https://doi.org/10.1002/srin.201900108.
[58] Shao L, Wang Q, Qu Y, Saxén H, Zou Z. A Numerical Study on the Operation of the H2 Shaft Furnace with Top Gas Recycling. Metall Mater Trans Bhttps://doi.org/10.1007/s11663-020-02020-6.
[59] Ranzani da Costa A, Wagner D, Patisson F. Modelling a new, low CO2 emissions, hydrogen steelmaking process. J Clean Prod 2013;46:27–35. https://doi.org/10.1016/J.JCLEPRO.2012.07.045.
[60] Kawasaki E, Sanscrainte J, Walsh TJ. Kinetics of reduction of iron oxide with carbon monoxide and hydrogen. AIChE J 1962;8(1):48–52. https://doi.org/10.1002/aic.690080114.
[61] Midrex. MIDREX Hotlink process.https://www.kobelco.co.jp/english/products/ironunit/dri/dri04.html.
[62] Duarte P, Pauluzzi D. Premium Quality DRI Products from ENERGIRON; 2019. https://www.energiron.com/wp-content/uploads/2019/05/Premium-Quality-DRI-Products-from-ENERGIRON.pdf.
[63] Pfeifer H, Kirschen M. Thermodynamic analysis of EAF energy efficiency and comparison with a statical model of electric energy model of demand. Engineering 2003:1–16.
[64] Kirschen M, Badr K, Pfeifer H. Influence of direct reduced iron on the energy balance of the electric arc furnace in steel industry. Energy 2011;36(10):6146–55. https://doi.org/10.1016/j.energy.2011.07.050.
[65] Catalan LJ, Rezaei E. Coupled hydrodynamic and kinetic model of liquid metal bubble reactor for hydrogen production by noncatalytic thermal decomposition of methane. Int J Hydrogen Energy 2020;45(4):2486–503. https://doi.org/10.1016/j.ijhydene.2019.11.143.
[66] Oleinik KI, Bykov AS, Pastukhov EA. Refinement of the thermophysical properties of liquid tin at high temperatures. Russian Metallurgy (Metally) 2018;2018(2):110–3. https://doi.org/10.1134/S0036029518020143.
[67] Assael MJ, Kalyva AE, Antoniadis KD, Michael Banish R, Egry I, Wu J, Kaschnitz E, Wakeham WA. Reference data for the density and viscosity of liquid copper and liquid tin. J Phys Chem Ref Data 2010;39(3):1–8. https://doi.org/10.1063/1.3467496.
[68] Ho MT, Bustamante A, Wiley DE. Comparison of CO2 capture economics for iron and steel mills. Int J Greenhouse Gas Control 2013;19:145–59. https://doi.org/10.1016/j.ijggc.2013.08.003.
[69] Gavin Towler RS. Chemical Engineering Design. 2nd ed. Elsevier; 2013. https://doi.org/10.1016/C2009-0-61216-2.
[70] Cihlar J, Lejarreta AV, Wang A, Melgar F, Jens J, Rio P, van der Leun K. Hydrogen generation in Europe: Overview of costs and key benefits, Tech. rep., European Commission, Luxembourg; 2020.https://doi.org/10.2833/122757.
[71] OECD. Steel Market Developments Q2 2020, Tech. Rep. June, OECD; 2020. URLhttps://www.oecd.org/sti/ind/steel-market-developments-Q2-2020.pdf.
[72] European Commission. Composition and Drivers of Energy Prices and Costs in Energy Intensive Industries., Tech. Rep. January, Directorate general for internal Market,Industry, Entrepreneurship and SMEs; 2018.https://doi.org/10.2873/004141.
[73] Cavaliere P. Direct Reduced Iron: Most Efficient Technologies for Greenhouse Emissions Abatement. In: Clean Ironmaking and Steelmaking Processes. Cham: Springer International Publishing; 2019. p. 419–84. https://doi.org/10.1007/978-3-030-21209-4_8.
[74] E. commission. Report from the commission to the European parliament and the council, report on the functioning of the European carbon market, Tech. rep., European commission, Brussels; 2020.
[75] Saltelli A, Annoni P, Azzini I, Campolongo F, Ratto M, Tarantola S. Variance based sensitivity analysis of model output. Design and estimator for the total sensitivity index. Comput Phys Commun 2010;181(2):259–70. https://doi.org/10.1016/j.cpc.2009.09.018.
[76] Hamby DM. A review of techniques for parameter sensitivity analysis of environmental models. Environ Monit Assess 1994;32(2):135–54. https://doi.org/10.1007/BF00547132.
[77] Sobol I. Global sensitivity indices for non-linear mathematical models and their Monte carlo estimates. Math Comput Simul 2001;5(2):271–80.
[78] Herman J, Usher W. SALib: an open-source python library for sensitivity analysis. J Open Source Software 2017;2(9):97. https://doi.org/10.21105/joss.00097.
[79] Bhaskar A. Material and energy balance model of the H-SF-EAF system using methane pyrolysis and water electrolysis; 2020.https://doi.org/10.5281/zenodo.4504841.
[80] Timmerberg S, Kaltschmitt M, Finkbeiner M. Hydrogen and hydrogen-derived fuels through methane decomposition of natural gas – GHG emissions and costs. Energy Convers Manage: X 2020;7(April):100043. https://doi.org/10.1016/j.ecmx.2020.100043.
[81] Moro A, Lonza L. Electricity carbon intensity in European Member States: Impacts on GHG emissions of electric vehicles, Transp Res Part D: Transp Environ 64 (July 2017) (2018) 5–14.https://doi.org/10.1016/j.trd.2017.07.012.
[82] Palmer C, Upham DC, Smart S, Gordon MJ, Metiu H, McFarland EW. Dry reforming of methane catalysed by molten metal alloys. Nat Catal 2020;3(1):83–9. https://doi.org/10.1038/s41929-019-0416-2.
[83] Mallapragada DS, Gençer E, Insinger P, Keith DW, O'Sullivan FM. Can industrial-scale solar hydrogen supplied from commodity technologies be cost competitive by 2030? Cell Reports Physical Science 2020:100174. https://doi.org/10.1016/j.xcrp.2020.100174.